Numerical simulation of thermal loading produced by shaped high power laser onto engine parts

Hong-Wei Song [a,*], Shao-Xia Li [a], Ling Zhang [a], Gang Yu [a], Liang Zhou [a], Jian-Song Tan [b]

[a] Institute of Mechanics, Chinese Academy of Sciences, Beijing 100190, PR China
[b] The College of Mechanical and Energy Engineering, Zhejiang University, Hangzhou 310027, PR China

ABSTRACT

Recently a new method for simulating the thermal loading on pistons of diesel engines was reported. The spatially shaped high power laser is employed as the heat source, and some preliminary experimental and numerical work was carried out. In this paper, a further effort was made to extend this simulation method to some other important engine parts such as cylinder heads. The incident Gaussian beam was transformed into concentric multi-circular patterns of specific intensity distributions, with the aid of diffractive optical elements (DOEs). By incorporating the appropriate repetitive laser pulses, the designed transient temperature fields and thermal loadings in the engine parts could be simulated. Thermal–structural numerical models for pistons and cylinder heads were built to predict the transient temperature and thermal stress. The models were also employed to find the optimal intensity distributions of the transformed laser beam that could produce the target transient temperature fields. Comparison of experimental and numerical results demonstrated that this systematic approach is effective in simulating the thermal loading on the engine parts.

© 2009 Elsevier Ltd. All rights reserved.

1. Introduction

Engine parts, include the pistons and cylinder heads, are subjected to severe thermal loading in service. The heat transfer process and thermal loading in an engine is however very complex. Firstly, combustion in the diesel engine is heterogeneous, and at any one time there are wide variations in gas temperatures through the charge. Secondly, periodic temperatures can be produced as the effect of the periodicity of engine cycles or of the unsteadiness of operating conditions corresponding to the driving cycle. The long-term thermal loading may result in fatigue on the engine parts. Thermal fatigue test on pistons and cylinder heads is therefore a very important step in evaluating the performance of diesel engines. Some experimental environments were developed to simulate the thermal loading and perform the thermal fatigue tests on various materials and structures, and these systems are usually based on localized flame, high frequency wire coil, thermal resistance, quartz lamp, etc. [1,2]. Recently high power laser was introduced to simulate the thermal loading on pistons [3,4]. Laser has been previously employed to study the thermal fatigue behavior of small material specimens cut from gas turbines, diesel engines, railroad steels, etc. [4–7]. However, it is difficult to perform thermal fatigue test on large workpieces, since laser is typically characterized by extreme focusing and directional irradiation at high energy density. With the aid of diffractive optical elements (DOEs), the incident Gaussian beam can be conveniently transformed into concentric multi-circular beams with specific intensity distribution. The spatially shaped intensity field, together with the temporally controlled repetitive laser pulses, may produce the transient temperature fields on the top surface of the piston similar to those in service.

In this paper, a further effort was made to extend this simulation method to some other important engine parts including cylinder heads. The transient temperature fields on pistons and those on cylinder heads are quite different. However, it has been sampled that the instantaneous temperature fields on the top surfaces of both parts are roughly in circular patterns in the normal working condition [8]. The advantage of laser as the heat source is that it can be designed flexibly in both spatial and temporal domain in controllable manners [4]. Therefore firstly one needs to find the optimal intensity distributions for the shaped beam that can produce appropriate temperature fields and thermal loadings for pistons and cylinder heads, respectively. Thermal–structural models were built to predict the transient temperature field and thermal stress in the engine parts when experienced periodical laser power, and the numerical models were validated by experiments. Then numerical models can not only be employed to find the optimal intensity field of shaped laser, but also serve as virtual experimental vehicles that greatly reduce the cost of thermal fatigue tests.

* Corresponding author. Tel.: +86 010 82544149.
E-mail address: songhw@imech.ac.cn (H.-W. Song).

2. Experimental

Fig. 1 gives the schematic of the experimental set-up. The system is consisted of three parts: the workbench, accessories, and system controls. The engine part being tested is deposited in the center of the workbench, overhead of which is a laser head. HAAS 3006D industrial Nd:YAG laser is employed to provide input energy with a power up to 3 kW. The laser beam was transformed into specific spatial intensity distributions with a DOE and irradiated on the top surface of the engine parts to impose an appropriate loading, as illustrated in Fig. 2. The DOEs were fabricated according to the optimal designs of intensity distribution for pistons and cylinder heads respectively, as illustrated in Fig. 3, and the design and fabrication process will be discussed in the coming sections. Infrared pyrometers (Model System 4, Land Instruments International) were mounted on the top of the workbench to sample the transient surface temperature at given regions. The response time is 100 ms, and the minimum target diameter is 3.5 mm. The pyrometers were adjusted by black-body material, and the emissivity of 0.48 was validated for the engine material (aluminum alloy). The repeatability and absolute measurement precisions are 1 °C and 4 °C, respectively. Three high resolution CCD cameras were used to sample images of the engine parts being tested. The main accessories are air compressor and water pump, which provide auxiliary cooling methods to the engine parts when necessary. System integration and control were accomplished by two PCs, based on Profibus-DP protocol.

The imposed thermal loading is controlled by two factors: the relative spatial intensity distribution $f(R)$ and the temporal profile of laser pulses $g(t)$. For both pistons and cylinder heads, the incident laser beam was transformed into concentric multi-circular patterns to obtain the desirable temperature fields. The transformed relative intensity field can be generalized into

$$f(R) = \begin{cases} \delta_i, & R \in [R_{i0}, R_{i1}] \\ 0, & R \notin [R_{i0}, R_{i1}] \end{cases} \qquad (1)$$
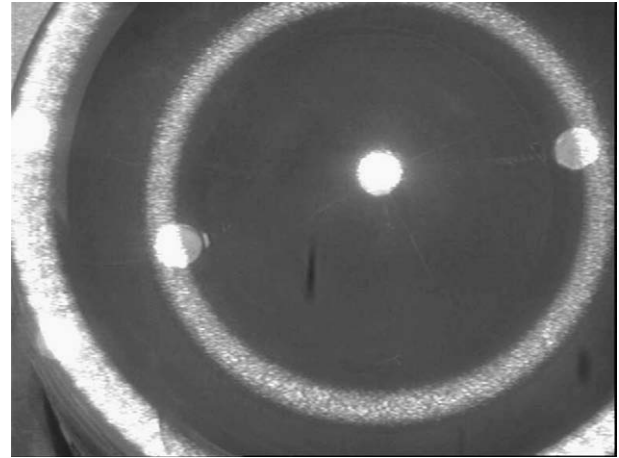

Fig. 2. Transformed laser beam with DOEs irradiated on the top surface of pistons.

where δ_i (i = 1–3) are the ratios of intensity between three laser irradiant circular bands, and the numbers 1, 2 and 3 indicate the center, middle and outer circular bands respectively. R_{i0} and R_{i1} (i = 1–3) are the inner radius and outer radius of the ith bands, respectively. Fig. 3 gives the final designs of transformed relative intensity fields for pistons and cylinder heads respectively, and both designs were obtained from numerical analysis. Notice that the center circular band of the transformed beam for the pistons shrinks into a spot. The temporal profile of the laser pulses $g(t)$ may be in diverse forms, taking repetitive square pulses as an example, it can be written into

$$g(t) = \begin{cases} P_h, & t \in [i(\tau_h + \tau_q), i(\tau_h + \tau_q) + \tau_q] \\ P_q, & t \in [i(\tau_h + \tau_q) + \tau_q, (i+1)(\tau_h + \tau_q)] \end{cases} \quad (i = 0, 1, 2, \ldots, n) \qquad (2)$$
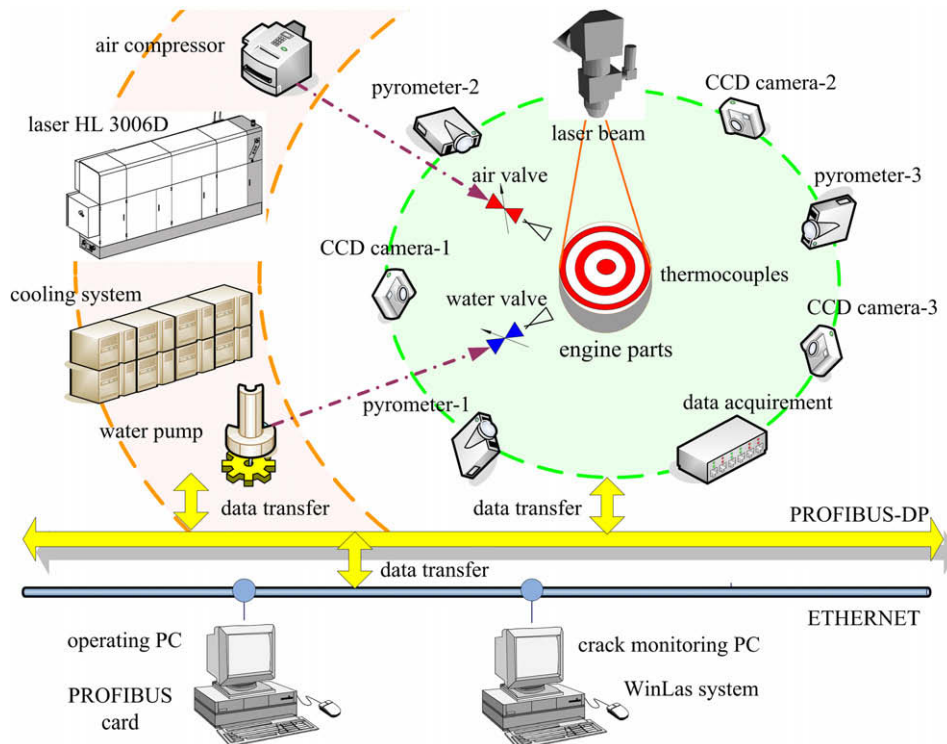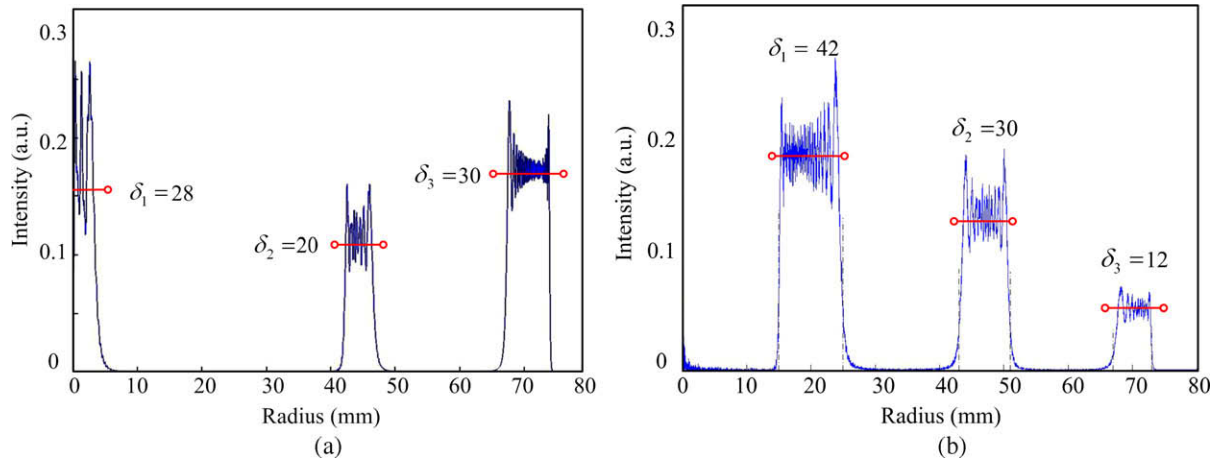

Fig. 1. Schematics of experimental set-up.

Fig. 3. Optimal designs of transformed relative intensity fields obtained from numerical analysis: (a) for pistons; (b) for cylinder heads.

where τ_h and τ_q are the heating duration and cooling duration in one thermal loading cycle, respectively; P_h and P_q are the laser powers at heating and cooling stages respectively. In the simulation test, the transformed laser beam produces spatial temperature gradient, whereas the temporal profile of laser pulses produces a heating period and a cooling period in one thermal cycle. The combination of $f(R)$ and $g(t)$ produces the imposed thermal load.

3. Design and fabrication of DOEs

Laser beam shaping is a technique that controls the irradiance and phase profile of the output laser [9]. In the present work, the laser beam was transformed by a kind of diffractive optical element (DOE) which is consisted of a refractive surface and a diffractive surface. Some references also denoted it as hybrid diffractive–refractive optical element. The surface relief microstructure of the DOE in the incident plane can be calculated from the target transformed intensity distribution in the irradiated plane (e.g., the optimal designs in Fig. 3, which are obtained from the numerical analysis), based on the energy conservation. Referring to Fig. 4, one obtains

$$I_{in}(r_{i1}^2 - r_{i0}^2) = I_0 \delta_i (R_{i1}^2 - R_{i0}^2) \tag{3}$$

where r_{i0} and r_{i1} are the inner radius and outer radius of the ith ($i = 1$–3) circular band in the incident plane. I_{in} is the power density

of incident laser beam, and I_{in} is assumed to be constant throughout the incident plane. I_0 is the unit power density of the shaped laser beam, which can be calculated from

$$I_0 = P \Big/ \sum \delta_i S_i \tag{4}$$

where S_i ($i = 1$–3) are the areas of irradiated bands by the shaped beam, P is the output laser power. Notice that in the present design method, $r_{i1} = r_{(i+1)0}$ and $r_{10} = 0$, therefore r_{i0} and r_{i1} can be solved one by one. Fig. 4 also gives

$$\frac{r^2 - r_{i0}^2}{r_{i1}^2 - r_{i0}^2} = \frac{R(r)^2 - R_{i0}^2}{R_{i1}^2 - R_{i0}^2} \tag{5}$$

According to the theory of diffractive optics, the phase profile can be written into

$$\frac{d\phi(r)}{dr} = \frac{2\pi}{\lambda} \frac{R(r) - r}{z} \tag{6}$$

Therefore

$$\frac{d\phi_i(r)}{dr} = \frac{2\pi}{\lambda} \frac{\sqrt{\frac{r^2 - r_{i0}^2}{r_{i1}^2 - r_{i0}^2}(R_{i1}^2 - R_{i0}^2) + R_{i0}^2} - r}{z} \tag{7}$$

where $\varphi_i(r)$ is the phase profile of the ith band in the DOE, λ is the wavelength, z is the distance between the incident plane (i.e., DOE plane) and the irradiated plane (i.e., the top surface of engine part). According to the phase profile, the minimum approaching sphere, or the focal length of the refractive surface can be calculated. Modulating the left phase, the phase profile of the diffractive surface can be obtained as well. The refractive surface was fabricated as the traditional transparent lens, whereas the diffractive surface was fabricated with the binary optics method. Therefore, the hybrid diffractive–refractive optical element that could transform the Gaussian laser beam into the designed intensity distribution was fabricated.

4. Thermal–structural analysis

4.1. Numerical model and intensity field design

Despite the complexity and heterogeneity in the combustion and heat transfer process of engine parts, in the normal working condition the temperature fields on the top surface of pistons and cylinder heads are basically in axisymmetric patterns [8]. For the ϕ 150 mm pistons made of aluminum alloy, the temperatures in the regions $\phi = 0$, 90 and 126 mm reach 300, 280 and 350 °C
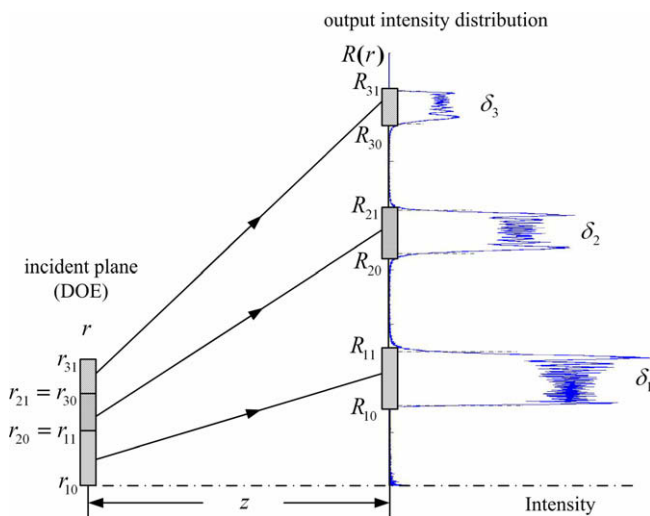

Fig. 4. Design of DOE according to the shaped output intensity distribution.

in the cooling period, then rise to 320, 290 and 360 °C respectively in the heating period. For the ϕ 150 mm cylinder heads, the temperatures in the regions ϕ = 44, 94 and 140 mm reach 170, 150 and 135 °C in the cooling period, then rise to 180, 160 and 140 °C respectively in the heating period. To simulate this behavior, the heat source should be designable in both spatial and temporal domain. Laser can achieve this goal. In the spatial domain, multi-circular patterns were designed for pistons and cylinder heads respectively, and the general expression can be found in Eq. (1). Given the values of R_{i0} and R_{i1} in $f(R)$, the optimal process turns to be finding the right values of δ_i that could obtain the target spatial temperature fields. In the temporal domain, the heating period and cooling period can be simulated by choosing the appropriate repetitive laser pulses, which were governed by $g(t)$ in Eq. (2).

A reverse method based on finite element model (FEM) has been proposed to acquire the optimal design for pistons [4]. In this method two major steps were incorporated: validation of FEM and optimization of intensity distribution. This method is as effective in designing the shaped intensity distribution for other engine parts, e.g., cylinder heads.

The geometry models of the piston and the cylinder head were built in the ProE environment and then exported into the commercial finite element package ANSYS. Compared to the piston, the geometry of cylinder head is much more complicated. In order to reduce the computational cost, some trivial geometries that are away from the laser irradiated regions, e.g., small sized holes, grooves and chamfers, were neglected in the cylinder head model. Meanwhile, meshes in the laser irradiated regions were refined to maintain sufficient accuracy. The transient temperature field $T(x,y,z,t)$ in the engine parts obeys the differential equation

$$\rho C \frac{\partial T}{\partial t} - k\nabla^2 T = 0 \tag{8}$$

where ρ, C and k are the density, specific heat and thermal conductivity, respectively, ∇^2 is the Laplacian operator. According to Fourier's law of heat conduction, the heat flux on the top surfaces of the engine parts obeys

$$q_z = -k\frac{\partial T}{\partial n} = A(T)f(R)g(t) \tag{9}$$

where $A(T)$ is the laser absorptivity, which is the ratio of the power absorbed at the surface to the output laser power at temperature T. The plane of symmetry and bottom surfaces are assumed to be thermal insulation, therefore they are assigned adiabatic boundary conduction. Surfaces besides the plane of symmetry and the bottom surfaces convect with the environment

$$-k\frac{\partial T}{\partial n}\bigg|_\Gamma = h(T - T_e) \tag{10}$$

where h is the coefficient of convection, T_e is the environmental temperature, n represents normal directions to the surface. By neglecting the pre-heating period, initial temperatures of sufficient high (for pistons, T_0 = 310 °C, for cylinder heads, T_0 = 150 °C) were assigned to the elements

$$T(x,y,z,0) = T_0 \tag{11}$$

This treatment significantly reduces the computational time as well. Three-dimensional temperature fields of the engine parts were obtained by solving the heat conduction problem with convective boundary conditions at the surfaces, governed by Eqs. (8)–(11). The numerical models were validated by the experiments carried out with a previously fabricated DOE. By approaching the computational results to the sampled temperatures in the laser irradiated areas, some important parameters including laser absorptivity, convective heat transfer coefficient and thermal conductivity were also validated.

The next step is optimizing the spatial intensity distribution of shaped beam. Iterative computational program based on the validated models was carried out to find the appropriate values for δ_i, therefore the target transient temperature fields could be reached when selecting the right loading case $g(t)$. The optimization process is ended when the transient temperature in each circular band is within 2 °C error compared to the target temperature. For the pistons, the optimal relative intensity field is δ_1 = 28, δ_2 = 20, δ_3 = 30, and R_{10} = 0, R_{11} = 4, R_{20} = 42, R_{21} = 47, R_{30} = 67 and R_{31} = 74 mm; whereas for the cylinder head, the optimal relative intensity field is δ_1 = 42, δ_2 = 30, δ_3 = 12, and R_{10} = 15, R_{11} = 25, R_{20} = 43, R_{21} = 51, R_{30} = 67 and R_{31} = 73 mm. The above two intensity distributions transformed with DOEs can be found in Fig. 3.

4.2. Transient temperature fields

The numerical and experimental results were compared in Fig. 5. The laser irradiated bands from inside to outside were denoted as center circular band, middle circular band and outer circular band respectively. In the experiment the infrared pyrometers sampled the temperature response of three characteristic spots in the center, middle and outer circular bands, till 100 thermal cycles (in one thermal cycle, $\tau_h = \tau_q$ = 2 s). The same loading case was applied to the numerical model. Fig. 5 gives the temperature responses from t = 200 to t = 400 s. The comparison shows that the overall temperature increase tendency, temperature gradient, and magnitude of temperature oscillation in each band obtained from the computational results agree well with those obtained from experiments. Therefore, the numerical method manifests reasonable reliability in designing the spatial intensity distribution of shaped laser beam. Fig. 5 also indicates that the transient temperature response approaches that of piston in normal working condition, stated at the beginning of this section.

Fig. 6 gives the computational temperature profiles of the piston and the cylinder head loaded by repetitive pulses of shaped laser transformed with the optimized DOEs. The temporal profiles of the loading cases, $g(t)$, are P_h = 2500 W, P_q = 500 W and $\tau_h = \tau_q$ = 2 s; P_h = 3000 W, P_q = 0 W and $\tau_h = \tau_q$ = 2 s, respectively. The figure simulates the temperature profiles at the end of heating period of high cycle fatigue tests.

Fig. 7 illustrates the evolution of temperature field on the top surface of the cylinder head in one thermal cycle. This thermal cycle is extracted from the end of 100 computed thermal cycles, when the temperature field reaches a dynamic equilibrium. The interval of each frame is 0.5 s. The heating period is t = 0–2 s, and the cooling period is t = 2–4 s. The temperature profile of the last frame (t = 3.5 s) is similar to that of the initial frame (t = 0 s), indicating a state of dynamic equilibrium. From the frames laser irradiated regions can be roughly seen, and they are characterized by three bands of relatively high temperature in the heating period. From numerical models one can obtain the temperature information in any region at any given loading step, and the instantaneous three-dimensional temperature field can be vividly demonstrated. By contrast, the experiments can provide temperature response of only limited regions. The computed results are also helpful in improving the experimental programs, thus greatly reduced the time and energy cost.

4.3. Thermal stress

Thermal stress is originated from the obstruction of deformation due to heterogeneous heating or cooling. Thermal stress and stress fluctuation in one thermal cycle can be computed by assigning appropriate boundary conditions and mechanical properties of materials, while using the results of thermal analysis as the load. The initial condition is assumed to be stress-free in the engine
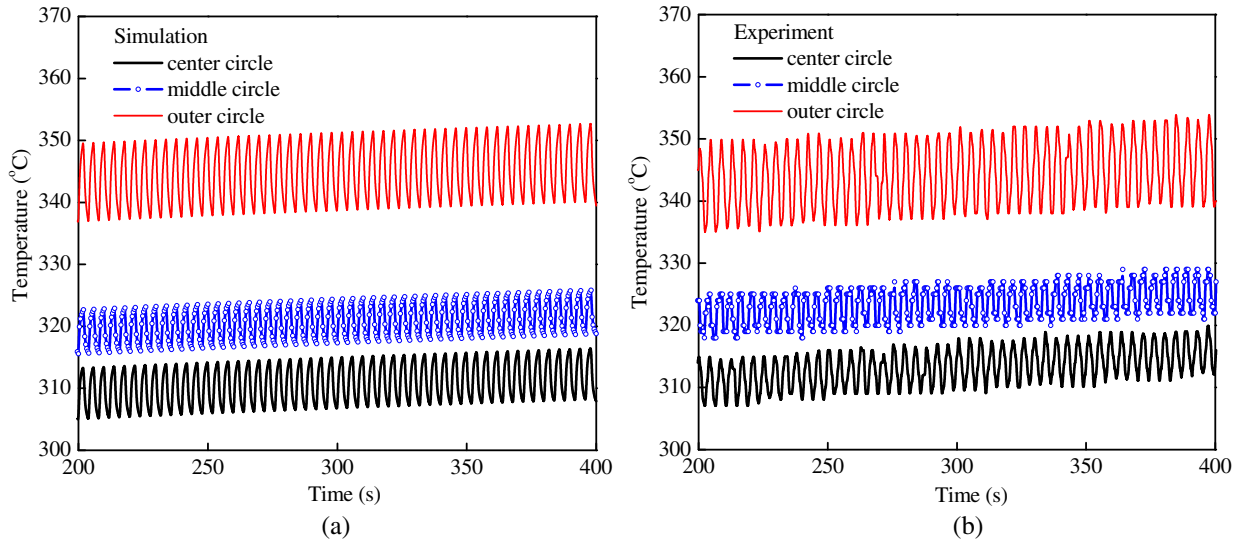
Fig. 5. Comparison of temperature response between numerical and experimental (a) simulation; (b) experiment.
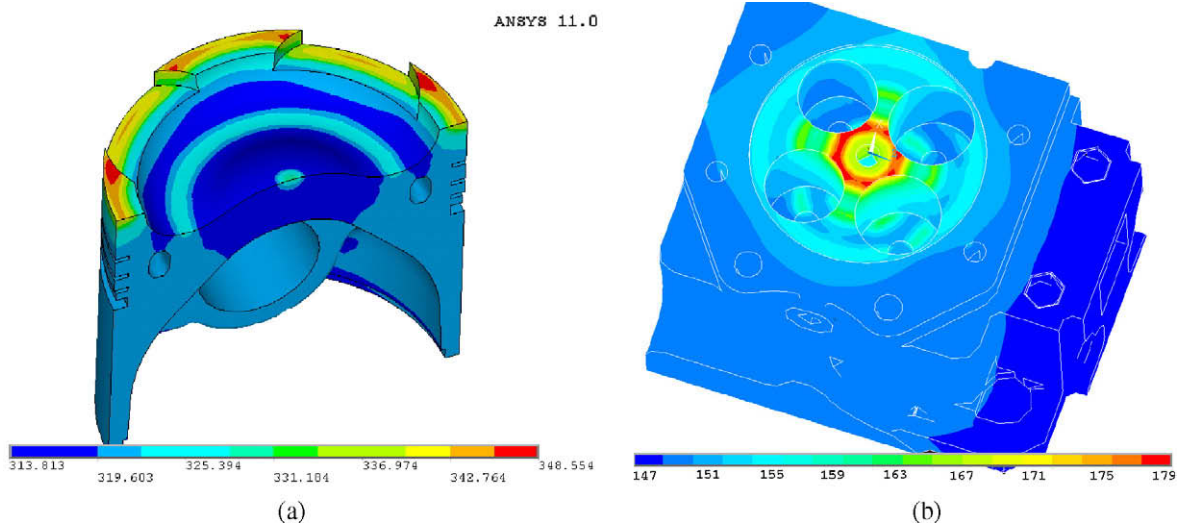

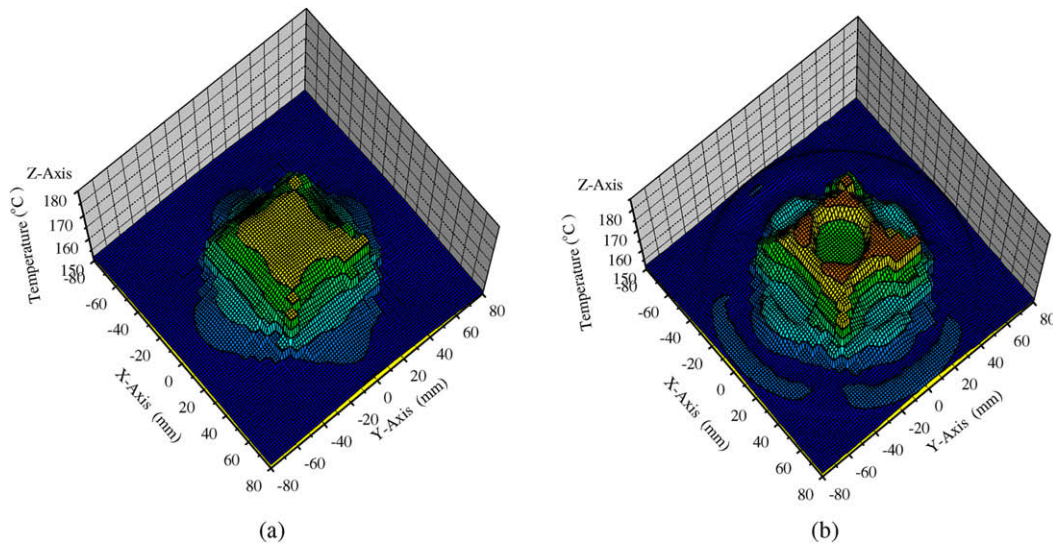**Fig. 6.** Computational temperature profiles (a) piston; (b) cylinder head.

Fig. 7. Transient temperature field on the top surface of cylinder head during one thermal cycle (a) t = 0 s; (b) t = 0.5 s; (c) t = 1.0 s; (d) t = 1.5 s; (e) t = 2.0 s; (f) t = 2.5 s; (g) t = 3.0 s; (h) t = 3.5 s.
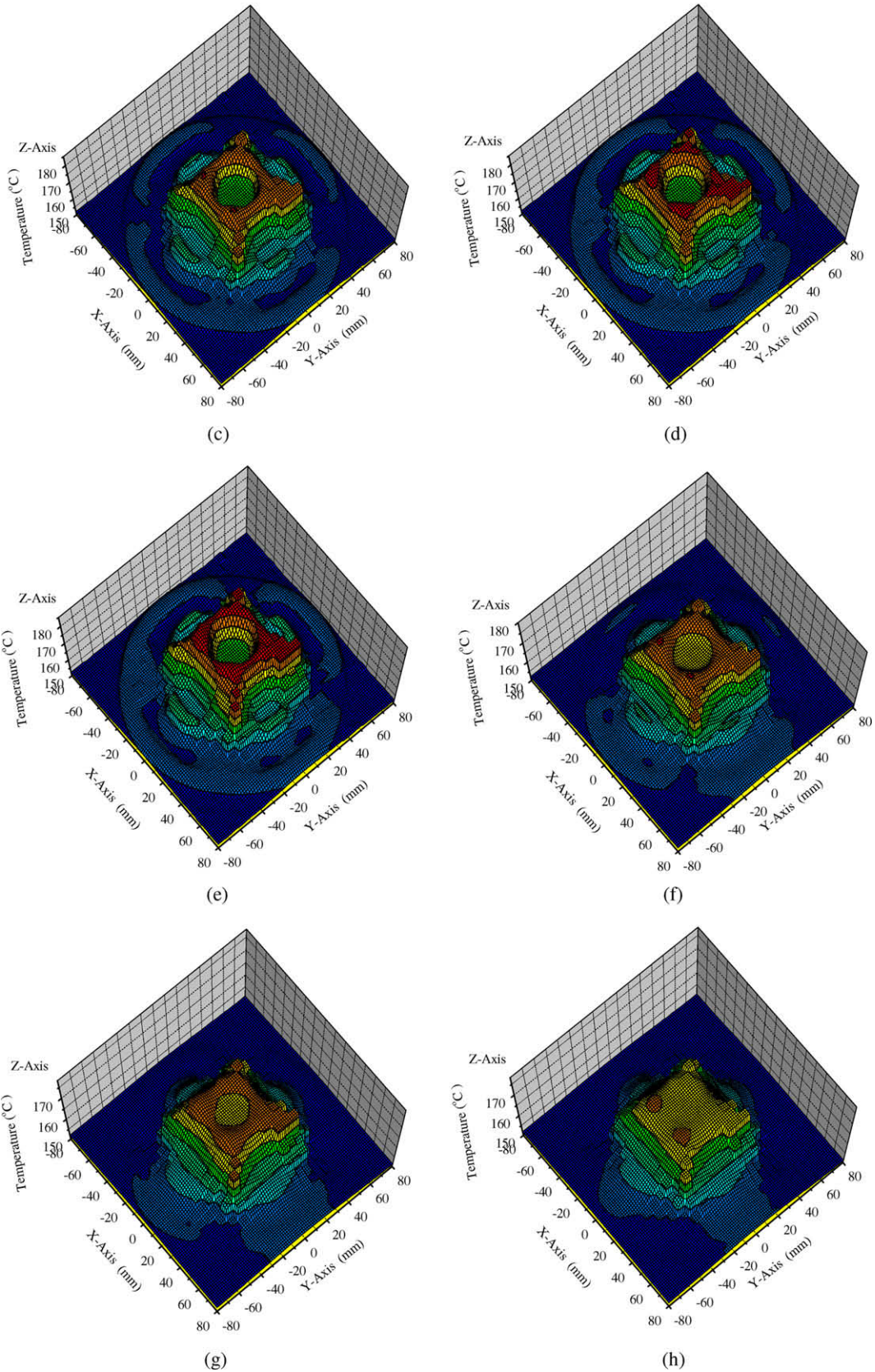
Fig. 7 (*continued*)

parts, and the bottom boundary of the structure is fully constrained. There is no displacement in the normal direction of the symmetry plane. The material for engine parts is aluminum alloy, and its thermal and mechanical properties are listed in Table 1.

Table 1
Thermal and mechanical properties of material for engine part.

Temperature (°C)	Elastic modulus E (GPa)	Yield strength σ_0 (MPa)	Tensile strength σ_u (MPa)	Thermal expansion coefficient α (1/$K \times 10^{-6}$)
20	80	230	250	21
150	77.3	220	230	21
250	72.5	110	150	21

For a thermo-elastoplastic problem, the total strain vector can be written in the incremental form

$$d\varepsilon_{ij} = d\varepsilon_{ij}^E + d\varepsilon_{ij}^P + d\varepsilon_{ij}^T \tag{12}$$

where $d\varepsilon_{ij}^E$, $d\varepsilon_{ij}^P$ and $d\varepsilon_{ij}^T$ are the incremental elastic strain vector, plastic strain vector and thermal strain vector, respectively. Materials expand or contract with temperature changes, therefore thermal strain depends on the present temperature and the initial temperature

$$d\varepsilon_{ij}^T = \alpha(\phi - \phi_0)\delta_{ij} \tag{13}$$

where α is thermal expansion coefficient, δ_{ij} is Kronecker delta, ϕ and ϕ_0 are the present temperature field and initial temperature field in the structure, respectively. The transient stress and strain responses are assumed to be quasi-static at each time interval, and the thermo-elastoplastic model is associated with the plastic flow rule and von Mises yielding criterion is used.

Fig. 8 illustrates the transient temperature and thermal stress in the piston subject to thermal shock, and the loading case is P_h = 2500 W, P_q = 0 W, τ_h = 35 s and τ_q = 25 s. Compressed air was applied on the top surface to introduce forced convection during the cooling period. At the end of heating cycle, the maximum compressive stress and tensile stress appears at the top surface of outer circle band and bottom surface of center circle band, respectively, and the value is about 80 and 30 MPa, respectively. At the end of cooling cycle, both the maximum compressive stress and the maximum tensile stress drop to below 20 MPa. The figure also indicate that the greatest variation in temperature and stress in one thermal cycle is in the outer circle band. Knowing the transient stress in the thermal cycles, thermal fatigue life-span therefore can be
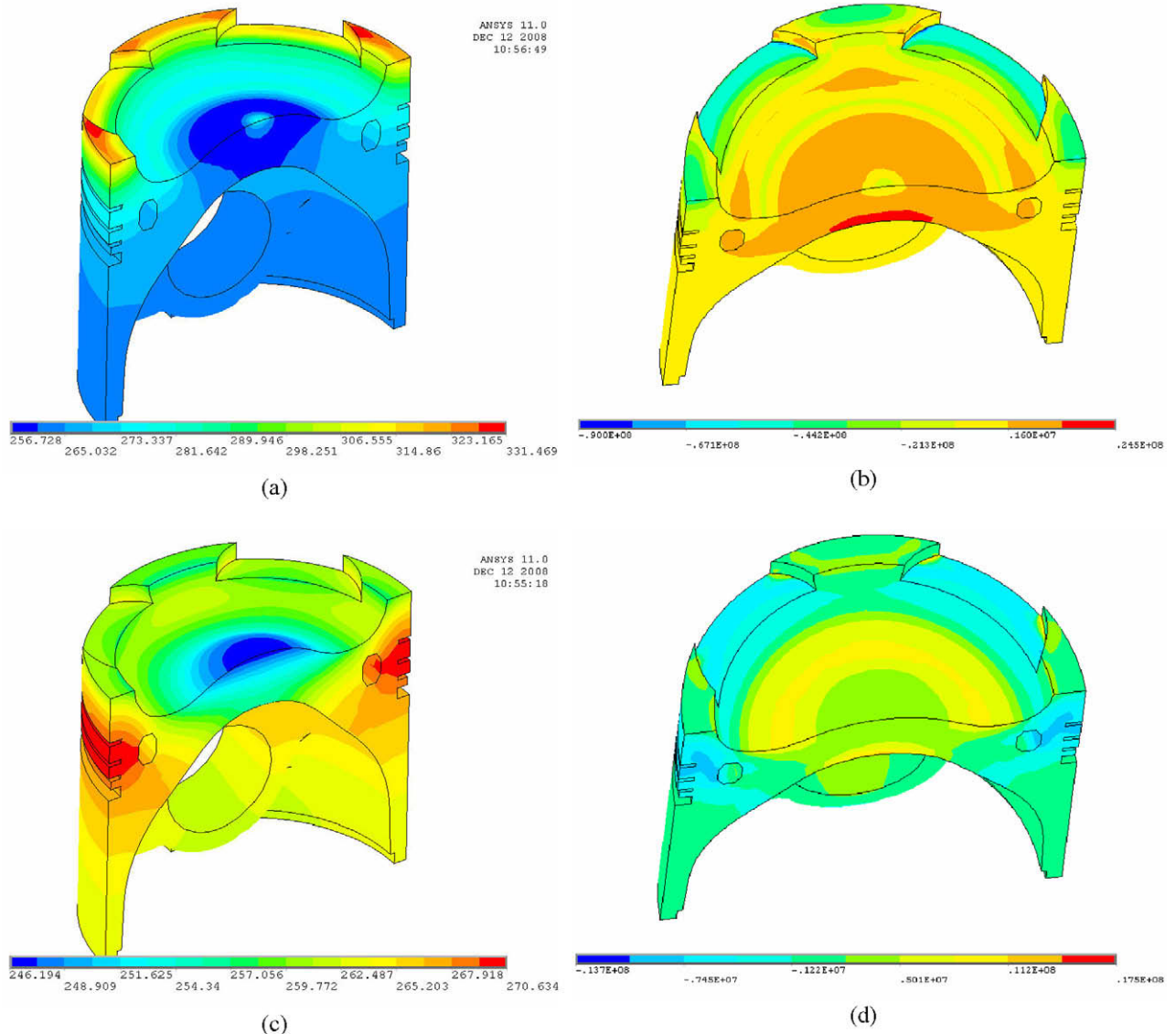

Fig. 8. Temperature and thermal stress of thermal shock on piston (a) temperature at the end of heating period; (b) hoop stress at the end of heating period; (c) temperature at the end of cooling period; (d) hoop stress at the end of cooling period.

calculated with the classic theory. The simulation environment may also be upgraded according to the analysis, e.g., enhance the thermal loading status by incorporating auxiliary cooling method including water and gas.

The above analysis demonstrates that the transformed high power laser is flexible in produce various thermal loadings. One can design different DOEs, alter the laser power P_h and P_q, and adjust the heating period τ_h and cooling period τ_q, to find the desirable loading cases. Actually the temperature distribution in the depth as well as thermal stresses depends on the amplitude and the frequency of the thermal load. When the laser power is sufficiently high, the heating cycle can be greatly reduced, and the cooling cycle can also be reduced with auxiliary cooling method.

5. Conclusions

The paper provides a numerical modeling of the thermal and structural response in engine parts while subjected to periodic thermal loading produced by shaped high power laser. The incident laser beam can be transformed into concentric multi-circular patterns of specific intensity distributions for pistons and cylinder heads respectively, through DOEs. By imposing appropriate laser loads, the transient temperature fields and thermal loadings in the engine parts could be simulated. Thermal–structural analysis for pistons and cylinder heads is an efficient way to predict the transient temperatures and thermal stresses, and the comparison of experimental and numerical results gave good agreement. The experimentally verified numerical models are also effective in the design of DOEs. This systematic approach is effective and flexible in simulating various thermal loadings on various engine parts.

Laser beam shaping technology has been nowadays used in a number of industrial sectors. However, use of the shaped laser beam to simulate the thermal loading on large engine parts like pistons and cylinder heads is still a new conception. Actually the intensity distribution of shaped laser beam for obtaining desired thermal response can be mathematically calculated in simple cases. Pistons and cylinder heads are large structures with complex configuration however, and the numerical method should be employed to deal with the complicated problems. The numerical models can also be employed as virtual experimental vehicles that reduce the cost of thermal fatigue tests.

Acknowledgements

References

[1] H.G. Baron, Thermal shock and thermal fatigue, in: P.P. Benham, R. Hoyle (Eds.), Thermal Stress, Sir Isaac Pitman & Sons Ltd., London, 1964, pp. 182–206.
[2] S.G. Long, Y.C. Zhou, Thermal fatigue of particle reinforced metal–matrix composite induced by laser heating and mechanical load, Composites Science and Technology 65 (2005) 1391–1400.
[3] H.W. Song, G. Yu, J.S. Tan, L. Zhou, X.L. Yu, Thermal fatigue on pistons induced by modulated high power laser. Part I: experimental study of transient temperature fields and temperature oscillations, International Journal of Heat and Mass Transfer 51 (2008) 757–767.
[4] H.W. Song, G. Yu, A.F.H. Kaplan, J.S. Tan, X.L. Yu, Thermal fatigue on pistons induced by modulated high power laser. Part II: design of spatial intensity distribution via numerical simulation, International Journal of Heat and Mass Transfer 51 (2008) 768–778.
[5] M. Schaus, M. Pohl, Nd-YAG-Laser simulated thermal shock and thermal fatigue behaviour of railroad steel, Metallurgy 52 (1998) 464–470.
[6] M. Kutsuna, S. Fujita, Y. Sugita, K. Yamada, Thermal fatigue test for turbine housing by a pulse YAG laser, in: High-Power Lasers in Manufacturing, Proceedings of SPIE 3888 (2000) 438–445.
[7] D.M. Zhu, D.S. Fox, R.A. Miller, L.J. Ghosn, S. Kalluri, Effect of surface impulsive thermal loads on fatigue behavior of constant volume propulsion engine combustor materials, Surface & Coatings Technology 188–189 (2004) 13–19.
[8] B. Challen, R. Baranescu, Diesel Engine Reference Book, second ed., Elsevier, 1999.
[9] F.M. Dickey, Laser beam shaping, Optics and Photonics News (2003) 31–34.